

Wideband Triple- and Quad-Resonance Substrate Integrated Waveguide Cavity-Backed Slot Antennas With Shorting Vias

Yuzhong Shi, Juhua Liu^{ID}, Member, IEEE, and Yunliang Long, Senior Member, IEEE

Abstract—A triple-resonance and a quad-resonance substrate integrated waveguide (SIW) cavity-backed slot antennas using shorting vias are presented in this paper. The antennas have wide bandwidths and low profiles. The working mechanism of the triple-resonance antenna is explained with its electric field distributions and equivalent circuit models. By loading the SIW cavity with shorting vias, the lowest mode (half-TE₁₁₀ mode) is shifted upward and coupled with two higher modes (even and odd TE₂₁₀ modes). As a result, a wide bandwidth with triple resonances is achieved for the antenna. Based on the similar principle, a quad-resonance antenna having an even wider bandwidth is also developed. Prototypes of the two antennas are fabricated and measured. With a low profile of $0.03\lambda_0$ (wavelength in free space), the triple-resonance design has a bandwidth of 15.2% and a peak gain of 4.80 dBi, and the quad-resonance design has a bandwidth of 17.5% and a peak gain of 7.27 dBi.

Index Terms—Cavity-backed slot antenna, shorting vias, substrate integrated waveguide (SIW), wideband.

I. INTRODUCTION

SUBSTRATE integrated waveguide (SIW) cavity-backed slot antennas show outstanding advantages (such as lightweight, low profile, and easy integration with planar circuits) in microwave and especially in millimeter-wave systems [1]–[11]. However, due to the high quality factor and single-resonance response, conventional SIW cavity-backed slot antennas usually suffer from narrow bandwidths (about 1.7% [1]), limiting their applications in broadband communication systems.

Recently, quite a few excellent works have been presented in the literature for enhancing the bandwidths of SIW cavity-backed slot antennas. In [2], the bandwidth was increased up to 2.16% by partial removal of the substrate. However, the bandwidth enhancement was limited because the design in [2] only utilized a single slot mode. Using additional resonant patch or slot, some wideband multimode SIW cavity-backed slot antennas were developed. In [3], a broadband

Manuscript received November 3, 2016; revised June 26, 2017; accepted September 15, 2017. Date of publication September 21, 2017; date of current version October 27, 2017. This work was supported in part by the Natural Science Foundation of China under Grant 61401522, Grant 61771497, Grant 41376041, and Grant 61172026 and in part by the NSF of Guangdong Province under Grant 2015A030312010. (*Corresponding author:* Juhua Liu.)

The authors are with the Department of Electronics and Communication Engineering, Sun Yat-sen University, Guangzhou 510006, China (e-mail: liuhj33@mail.sysu.edu.cn).

Color versions of one or more of the figures in this paper are available online at <http://ieeexplore.ieee.org>.

Digital Object Identifier 10.1109/TAP.2017.2755118

SIW cavity-backed patch antenna was proposed, in which an additional patch mode and a cavity TE₂₁₀ mode were excited. In [4], a dual-resonance slot-patch structure composed of a half-wavelength slot and a parasitic patch was employed for bandwidth enhancement. In [5], a wideband dual-mode design using triangular complimentary split ring slot (TCSRS) achieved a bandwidth of 16.7%. Several dual-band SIW cavity-backed slot antennas were also realized with specific slot shapes (e.g., dumbbell-shaped slot [6], dual rectangular slot [7], and triangular-ring slot [8]).

In [9], by dividing an SIW cavity into two half parts with a nonresonant rectangular slot, two hybrid cavity modes were excited, and the fractional bandwidth could be improved up to 6.3%. Based on the similar principle, the SIW cavity antenna in [10] achieved a wider bandwidth of 9.4% using a bowtie-shaped slot. In [11], an SIW cavity-backed 3×3 slot array antenna was studied. Three high-order cavity modes (TE₁₃₀, TE₃₁₀, and TE₃₃₀) along with the slot mode were utilized in this design, leading to a bandwidth over 26%.

Previously, shorting vias were introduced in SIW-based feeding networks for improving the impedance matching of the antennas in [12] and [14]. In [15], a dual-resonance SIW cavity-backed slot antenna was realized using a via hole above the slot. Nevertheless, the bandwidth of the antenna in [15] was comparatively narrow (3.3%). Shorting vias were also used in SIW filters [16], [17], SIW frequency selective surface [18], and patch antennas [19], [20] for bandwidth enhancement.

In this paper, we propose two wideband SIW cavity-backed slot antennas using shorting vias. The two antennas have triple and quad resonances in their operation bands, respectively. The triple-resonance antenna is analyzed with its field distributions and equivalent circuit models. With the shorting vias loading, the lowest mode in the SIW cavity is shifted upward and coupled with two higher order modes. Therefore, a wide bandwidth with triple resonances is realized. The triple-resonance antenna has a very low profile of $0.03\lambda_0$ and a measured bandwidth of 15.2%. With the similar method, a quad-resonance antenna is also designed. By utilizing an additional resonance mode, the quad-resonance antenna achieves a wider bandwidth of 17.5%. The two antennas have stable radiation patterns and flat gains in their operation bands.

II. TRIPLE-RESONANCE ANTENNA

A. Geometry

Fig. 1 shows the geometry of the proposed triple-resonance antenna. The antenna is constructed on a single-layer substrate

0018-926X © 2017 IEEE. Personal use is permitted, but republication/redistribution requires IEEE permission.
See http://www.ieee.org/publications_standards/publications/rights/index.html for more information.

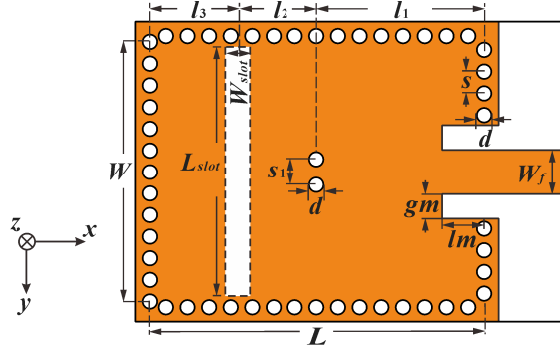


Fig. 1. Configuration of the proposed triple-resonance antenna.

TABLE I
DIMENSIONAL PARAMETERS FOR THE PROPOSED ANTENNAS

Parameter	Non-loaded dual-band antenna (Fig. 3)	Via-loaded triple-resonance antenna (Fig. 1)	Via-loaded quad-resonance antenna (Fig. 11)
W	18.8 mm	18.8 mm	18.8 mm
L	23.2 mm	23.2 mm	33 mm
W_{slot}	0.5 mm	1.1 mm	1.5 mm
L_{slot}	17.7 mm	17.7 mm	17.7 mm
l_4			5.8 mm
l_3	5.6 mm	6.0 mm	5.7 mm
l_2	$l_1 + l_2 = 17.6$ mm	5.6 mm	10.7 mm
l_1		11.6 mm	10.8 mm
s_2			1.35 mm
s_1	1.8 mm	1.8 mm	1.2 mm
s	1.5 mm	1.5 mm	1.5 mm
d	1.0 mm	1.0 mm	1.0 mm
g_m	1.2 mm	1.7 mm	1.6 mm
l_m	2.9 mm	2.9 mm	2.5 mm
W_f	3.1 mm	3.1 mm	3.1 mm
h	1.0 mm	1.0 mm	1.0 mm
ϵ_r	2.2	2.2	2.2

with a thickness of h and a relative permittivity of ϵ_r . Arrays of grounded vias are uniformly distributed along the edges of the antenna to build an SIW cavity. In order to avoid the energy leakage from the via gaps, the diameter d and the spacing of the sidewall shorting vias s are chosen to be $d = 1$ mm and $s = 1.5$ mm, respectively, which satisfy the conditions of $s/d \leq 2$ and $d/\lambda_0 \leq 0.1$ [21], [22]. Another two shorting vias with the same diameter d and a spacing s_1 are inserted near the center of the SIW cavity. A rectangular slot is etched on the ground plane for radiation. Here, the slot has a length of more than $\lambda_0/2$, and therefore it is a nonresonant slot [9]. A 50Ω microstrip line is used to feed the antenna. Detailed dimensional parameters are listed in Table I.

B. Antenna Without Shorting Vias

In order to reveal the loading effects of shorting vias, the cavity slot antenna without shorting vias is simulated using HFSS at first. The dimensional parameters of the non-loaded antenna are given in Table I. Fig. 2 shows the simulated input resistance (real part of the input impedance) and reflection coefficient. Three different working modes can be distinguished from the input resistance curve. The electric field

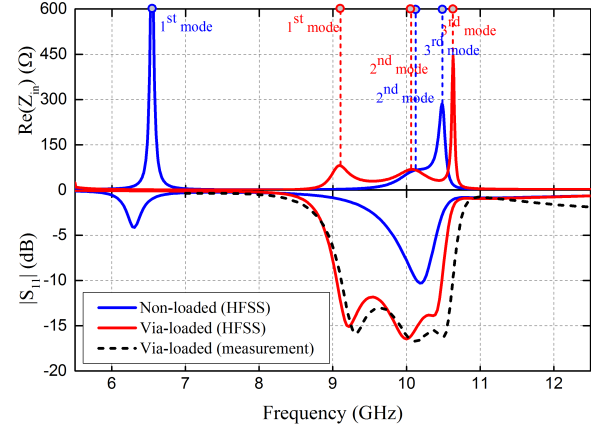


Fig. 2. Input resistances and reflection coefficients of the antennas with and without shorting vias. Different modes are distinguished from the peaks of the input resistance curves.

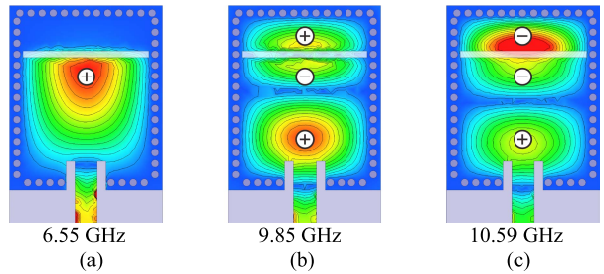


Fig. 3. Electric field distributions simulated from HFSS for the non-loaded antenna working in (a) half-TE₁₁₀ mode, (b) odd TE₂₁₀ mode, and (c) even TE₂₁₀ mode.

distributions of the three modes are shown in Fig. 3(a)–(c). Fig. 3(a) depicts the electric field distribution of the first mode at 6.55 GHz. This mode is defined as half-TE₁₁₀ mode [23]. Fig. 3(b) and (c) represent the electric field distributions of the two higher order modes at 9.85 and 10.59 GHz, respectively. These two modes are defined as odd TE₂₁₀ and even TE₂₁₀ modes, since their electric field distributions show odd and even symmetries around the slot, respectively.

As shown in Fig. 2, by merging the two higher modes, a bandwidth of 9.1% (9.64–10.55 GHz) is obtained for the upper band. However, it is still very difficult for this non-loaded antenna to combine the three modes together to generate a wider bandwidth, because the resonant frequency of the lowest half-TE₁₁₀ mode is far lower than those of the two higher modes.

C. Antenna With Shorting Vias

As indicated by the simulated input resistance shown in Fig. 2, when the shorting vias are employed, the resonant frequency of the lowest mode is shifted upward and the three modes are merged within a wide frequency range.

The field distributions of the three modes in the via-loaded antenna are shown in Fig. 4(a)–(c). On one hand, it is seen from Fig. 4(a) that the half-TE₁₁₀ mode is greatly perturbed by the shorting vias, which results in an upward shifting effect of its resonant frequency. On the other hand, the field

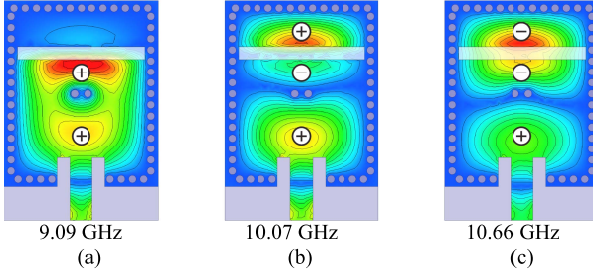


Fig. 4. Electric field distributions simulated from HFSS for the via-loaded antenna working in (a) half-TE₁₁₀ mode, (b) odd TE₂₁₀ mode, and (c) even TE₂₁₀ mode.

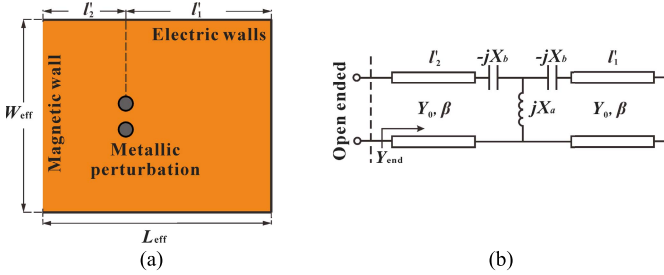


Fig. 5. (a) Equivalent cavity model and (b) equivalent circuit model for the proposed SIW cavity slot antenna working in the half-TE₁₁₀ mode.

distributions for the odd and even TE₂₁₀ modes remain almost unchanged with the shorting vias loading, since the shorting vias here are placed at the null-voltage point of these two higher modes. As a result, the resonant frequencies of the odd and even TE₂₁₀ modes are almost the same as those of the non-loaded antenna. Therefore, the three modes can be combined to achieve a wider bandwidth. As seen from the reflection coefficients shown in Fig. 2, the via-loaded antenna has a simulated fractional bandwidth of 14.9% (9.04–10.50 GHz), with an increase of 5.8% compared to that of the non-loaded one.

The radiation of the antenna is generated by the transverse electric field across the slot [9]. The half-TE₁₁₀ and odd TE₂₁₀ modes are radiating modes, but not the even TE₂₁₀ mode, since both sides of the slot for the even mode have the same voltage [Fig. 4(c)]. Fortunately, the resonant frequency of the nonradiating even TE₂₁₀ mode (10.66 GHz) is outside of the operation band (from 9.04 to 10.50 GHz). Therefore, the antenna can utilize the nonradiating mode for bandwidth enhancement while retaining stable radiation in the operation band.

III. EQUIVALENT CIRCUIT MODELS

In order to explain the working principles of the triple-resonance antenna more clearly, equivalent circuit models for the three different working modes are provided in this section for approximate analyses.

A. Half-TE₁₁₀ Mode

The proposed antenna working in the half-TE₁₁₀ mode [Fig. 4(a)] can be approximated as a quarter-wavelength cavity model, as shown in Fig. 5(a). The equivalent cavity is bounded by a magnetic wall at the open end and three electric walls at

the other three sides. Note that the microstrip feeding structure is eliminated for simplifying the analysis. The width of the cavity model can be approximately calculated by [24]

$$W_{\text{eff}} = W - \frac{d^2}{0.95s}. \quad (1)$$

As shown in Fig. 5(a), the cavity can be divided into two sections, and the length of the cavity becomes

$$L_{\text{eff}} = l'_1 + l'_2 \quad (2)$$

where l'_1 and l'_2 denote the lengths of the two SIW sections. They can be calculated by

$$l'_1 = l_1 - \frac{0.5d^2}{0.95s} \quad (3)$$

and

$$l'_2 = l_2 + \Delta l - \frac{W_{\text{slot}}}{2} \quad (4)$$

where Δl is the effective extension characterizing the effect of the fringing field at the open end. The extension Δl can be approximately calculated by [25]

$$\Delta l = 0.412h \frac{(\epsilon_r + 0.3)(W_{\text{eff}}/h + 0.264)}{(\epsilon_r - 0.258)(W_{\text{eff}}/h + 0.8)}. \quad (5)$$

Based on the cavity model, an equivalent circuit model [Fig. 5(b)] is introduced for the antenna working in the half-TE₁₁₀ mode. In this equivalent circuit, the characteristic admittance Y_0 and phase constant β of the SIW transmission line can be calculated by

$$Y_0 = \frac{\beta}{\eta_0 k_0} \frac{W_{\text{eff}}}{h} \quad (6)$$

and

$$\beta = \sqrt{k_0^2 \epsilon_r - \left(\frac{\pi}{W_{\text{eff}}} \right)^2} \quad (7)$$

where k_0 and $\eta_0 = 120\pi$ are the wavenumber and wave impedance in free space, respectively.

The loading via array can be modeled as a *C-L-C* T-network [26], which characterizes the inductive loading effect of the shorting vias and the coupling effect between the two SIW sections. Since the spacing between the shorting vias is very small ($s_1 \ll \lambda_0$), the electric field between the pair of shorting vias could be approximately neglected. Then, the via array [Fig. 6(a)] can be further approximated with a solid elliptic metallic post [Fig. 6(b)], in which the major axis d' and minor axis d'' are given by

$$d' = s_1 + d \quad (8)$$

and

$$d'' = d. \quad (9)$$

Then, the reactances X_a and X_b in Fig. 5(b) can be calculated by the expressions for the elliptic metallic post [26], namely

$$X_b = \frac{\beta \pi d''}{4Y_0 W_{\text{eff}}} (d' + d'') \quad (10)$$

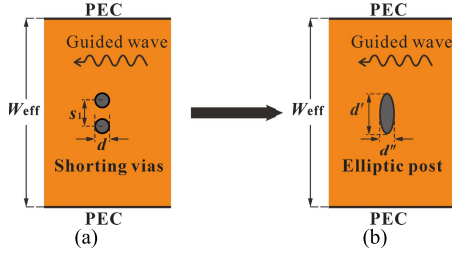


Fig. 6. (a) Shorting-via array in the SIW cavity and (b) its approximation using elliptic metallic post.

TABLE II

CALCULATED AND SIMULATED RESONANT FREQUENCIES
FOR THE HALF-TE₁₁₀ MODE IN THE ANTENNAS
WITH DIFFERENT VIA SPACINGS

Via spacing s_1 (mm)	Simulated (GHz)	Calculated (GHz)	Error (%)
Non-loaded	6.55	6.34	3.21
1	8.83	9.13	3.40
1.4	8.96	9.29	3.68
1.8	9.08	9.42	3.74
2.2	9.19	9.56	4.02
2.6	9.29	9.69	4.30
3	9.37	9.81	4.70

and

$$X_a = \frac{X_b}{2} + \frac{W_{\text{eff}}\beta}{4\pi Y_0} \times \left\{ \ln \frac{8W_{\text{eff}}}{\pi(d' + d'')} - 2 + \sum_{n=2}^{\infty} 2 \sin^2 \frac{n\pi}{2} \right. \\ \left. \times \left[\frac{1}{\sqrt{n^2 - \left(\frac{k_0 W_{\text{eff}}}{\pi} \right)^2}} - \frac{1}{n} \right] \right\}. \quad (11)$$

When the antenna is in resonance, the terminal admittance Y_{end} seen from the open end should be zero, namely

$$Y_{\text{end}} = 0. \quad (12)$$

Using the above equations, the resonant frequencies of the half-TE₁₁₀ modes in the antennas with and without shorting vias can be theoretically calculated. Table II shows the theoretical results in comparison with the simulated ones for the antennas with different via spacings (s_1). First, both the theoretical calculation and simulation indicate that the resonant frequency of the half-TE₁₁₀ mode is shifted upward by loading shorting vias. Second, it is seen that the increase of the via spacing s_1 leads to a higher resonant frequency of the half-TE₁₁₀ mode. Third, the theoretical calculation exhibits a good prediction of the resonant frequency with a relative error of less than 4.7% for $1 \text{ mm} \leq s_1 \leq 3 \text{ mm}$. In the case of our proposed design ($s_1 = 1.8 \text{ mm}$), the relative error is 3.74%, which is reasonable.

B. Even and Odd TE₂₁₀ Modes

The equivalent cavity model and circuit model for the proposed antenna working in the TE₂₁₀ modes are shown

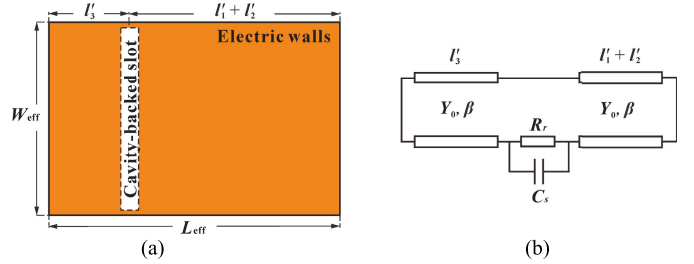


Fig. 7. (a) Equivalent cavity model and (b) equivalent circuit model for the proposed SIW cavity slot antenna working in the TE₂₁₀ mode.

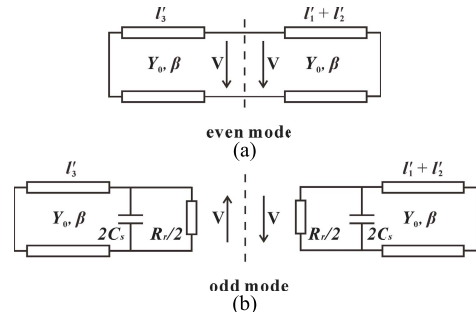


Fig. 8. Equivalent circuit models for the antenna working in (a) even TE₂₁₀ mode and (b) odd TE₂₁₀ mode. The voltage polarities on the edges of the cavity-backed slot are characterized with the symbol "V".

in Fig. 7(a) and (b), respectively. Note that the loading via array is removed from the cavity model for simplicity, since the vias are placed at the null-voltage point of the two TE₂₁₀ modes, as stated in Section II-C.

In the equivalent circuit model [Fig. 7(b)], the cavity-backed slot is modeled as a parallel connection of a resistance R_r and a capacitance C_s . The resistance R_r represents the radiation effect of the slot, while the capacitance C_s characterizes the coupling effect between the two SIW sections [Fig. 7(a)]. Next, we consider the even mode and the odd mode separately.

For the even TE₂₁₀ mode, the adjacent edges of the two SIW sections have equal voltage. In this case, the capacitance C_s and the resistance R_r do not load the circuit [27], and the modified circuit model for this mode is shown in Fig. 8(a).

For the odd TE₂₁₀ mode, on the other hand, the voltages on the adjacent edges of the two SIW sections are out of phase, and a voltage null appears at the midplane of the slot. Hence, the circuit can be bisected by grounding the midplane of the slot, and a modified circuit model for the odd mode can be obtained [27], as shown in Fig. 8(b). With the capacitance loading, the resonant frequency of the odd TE₂₁₀ mode is inevitably lower than that of the even TE₂₁₀ mode. This theoretical analysis is consistent with the simulation using HFSS.

The proposed antenna can also be considered as an integration of a slot antenna with a triple-mode SIW cavity filter. From this point of view, the wideband triple-resonance response of the antenna is provided by the integrated SIW cavity filter. This principle is similar to those multi-resonance SIW filtering antennas in [28]–[30].

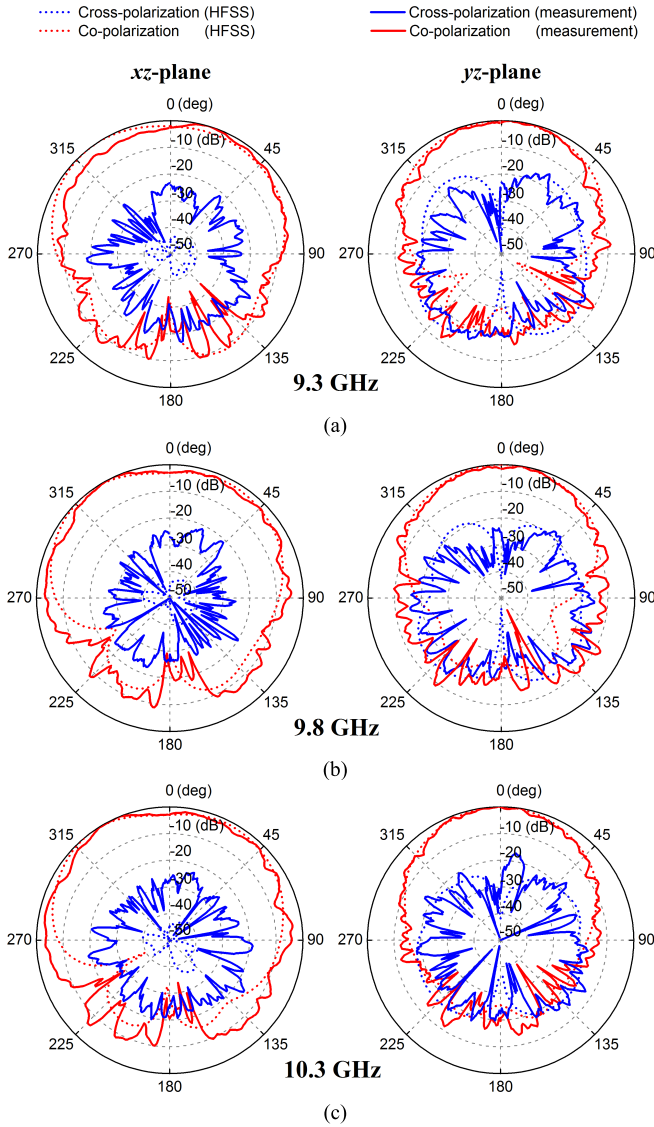


Fig. 9. Simulated and measured normalized radiation patterns of the proposed triple-resonance antenna. (a) 9.3 GHz. (b) 9.8 GHz. (c) 10.3 GHz.

IV. EXPERIMENT FOR TRIPLE-RESONANCE ANTENNA

A prototype of the triple-resonance design is fabricated on a Wang-Ling F4BMX220 substrate with a thickness of $h = 1$ mm, a relative permittivity of $\epsilon_r = 2.2$, and a loss tangent of $\tan\delta = 0.001$. Detailed dimensional parameters for the fabricated antenna are listed in Table I. The top and bottom views of the fabricated antenna are shown by the insets in Fig. 10.

The measured reflection coefficient ($|S_{11}|$) of the fabricated antenna is shown in Fig. 2. It is seen that the measured result agrees well with the simulated one from HFSS. The measured result shows that the antenna has a 10 dB impedance bandwidth of 15.2%, ranging from 9.12 to 10.62 GHz.

Fig. 9 shows the normalized radiation patterns at 9.3, 9.8, and 10.3 GHz for the antenna. The measured results are in good agreement with the simulated results. Both the simulation and measurement show that the radiation patterns are stable in the operation band, because the radiation can only be

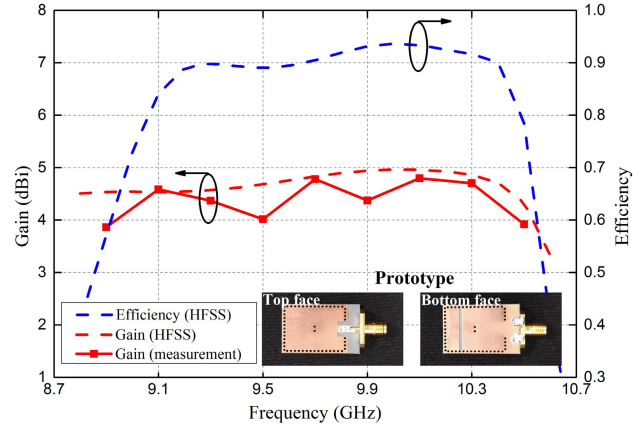


Fig. 10. Gain and efficiency of the proposed triple-resonance antenna.

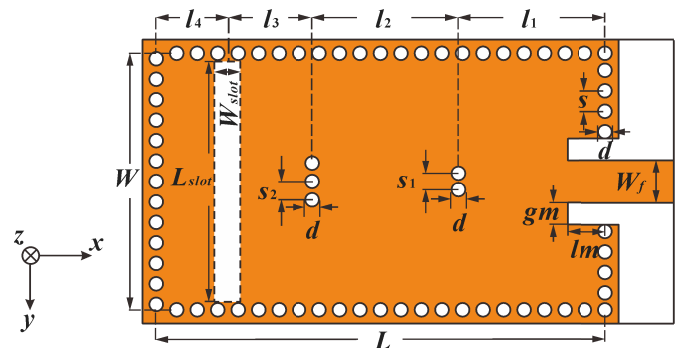


Fig. 11. Configuration of the proposed quad-resonance antenna.

emitted from the slot aperture and the transverse electric field across the slot maintains stable. In the upper half-space, the measured results show that the cross-polarization levels are about -20 dB.

Fig. 10 shows the measured gain in comparison with the simulated result. The measured gain is slightly (less than 1 dB) lower than the simulated one, probably due to the measurement error and the additional loss introduced by the sub-miniature version A connector. In the band of interest, the antenna has a flat gain with a measured peak value of 4.80 dBi and a variation range within 1 dB. In Fig. 10, the simulated efficiency of the antenna is also shown, and a peak efficiency of 93.6% is observed.

V. QUAD-RESONANCE ANTENNA

In order to further enlarge the bandwidth, a quad-resonance antenna (shown in Fig. 11) is developed in this section. Compared with the triple-resonance antenna, the quad-resonance antenna is designed to excite one more cavity mode (TE_{310} mode). In addition, two rows of shorting vias are inserted at the null-voltage points of the TE_{310} mode. The numbers and via spacings of the two rows of shorting vias have been chosen properly for an optimal bandwidth. The electric field distributions for the four modes are shown in Fig. 12. It is seen that the lower three resonance modes (the half- TE_{110} mode, even TE_{210} mode, and odd TE_{210} mode) are perturbed, while the TE_{310} mode remains almost unchanged.

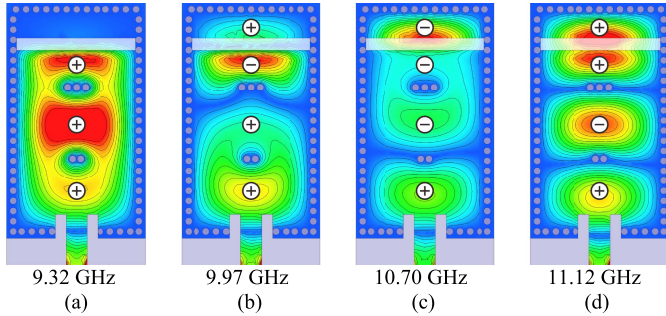


Fig. 12. Electric field distributions simulated from HFSS for the proposed quad-resonance antenna working in (a) half-TE₁₁₀ mode, (b) odd TE₂₁₀ mode, (c) even TE₂₁₀ mode, and (d) TE₃₁₀ mode.

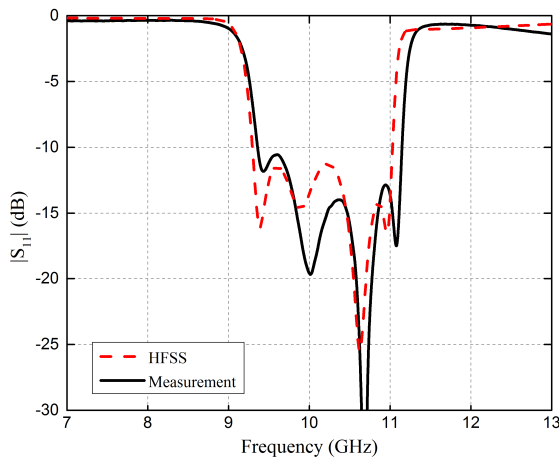


Fig. 13. Simulated and measured reflection coefficients of the proposed quad-resonance antenna.

Similar to the working mechanism of the triple-resonance antenna, the shoring vias here also have an upward shifting effect on the lower three modes. Therefore, the four resonance modes of the quad-resonance antenna can be merged to generate a wider bandwidth. To validate the design concept, a prototype of the quad-resonance antenna is fabricated, as shown by the insets in Fig. 15. Detailed dimensional parameters of the antenna are listed in Table I.

Fig. 13 shows the simulated and measured reflection coefficients of the quad-resonance antenna. It is obviously seen that four resonance modes are excited. The measured result shows that the antenna has a reflection coefficient below -10 dB from 9.36 to 11.26 GHz, with a wide fractional bandwidth of 17.5%.

Fig. 14 illustrates the radiation patterns of the quad-resonance design at 9.5, 10, and 10.5 GHz. It is seen that the measured patterns are close to the simulated ones, despite the small discrepancies (especially in the backward direction) caused by the experimental tolerances and imperfections [31]. Similar to the triple-resonance antenna, the quad-resonance antenna here also has stable radiation patterns with the main beam in the broadside direction. A low cross-polarization level of about -20 dB is observed.

Fig. 15 shows the efficiency and gain of the antenna. The simulated efficiency reaches a peak value of 94.2% at 10.6 GHz. The measured gain is stable, with a peak gain

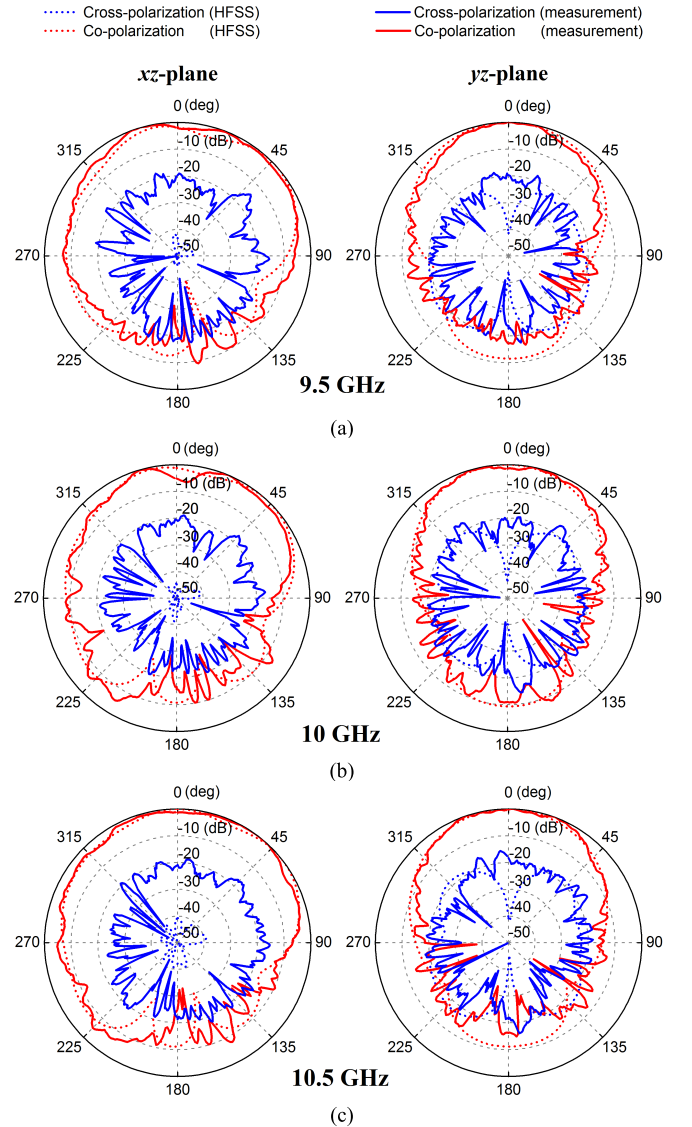


Fig. 14. Simulated and measured normalized radiation patterns of the proposed quad-resonance antenna. (a) 9.5 GHz. (b) 10 GHz. (c) 10.5 GHz.

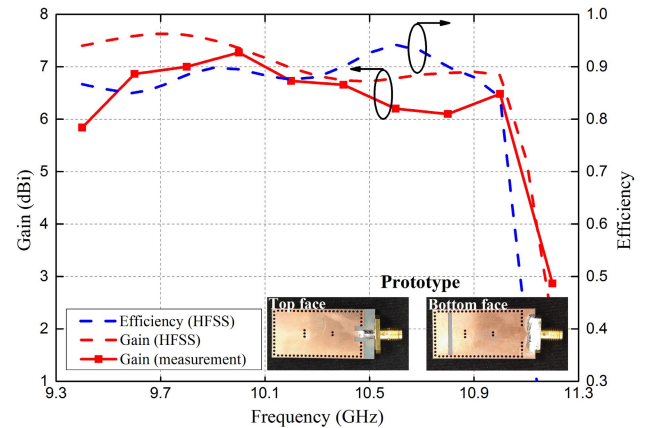


Fig. 15. Gain and efficiency of the proposed quad-resonance antenna.

of 7.27 dBi and a gain variation within 1.5 dB from 9.4 to 11 GHz. In this antenna, the TE₃₁₀ mode is a nonradiating mode, since it is an even mode with respect to the slot.

TABLE III
COMPARISON OF DIFFERENT SIW CAVITY-BACKED ANTENNAS

Antennas	Operating frequency (GHz)	ε_r	Dimension	10-dB BW	Peak gain (dBi)	Simulated peak efficiency	Feed type
Triple-resonance SIW CBS* antenna in this work	10	2.2	$0.63\lambda_0 \times 0.77\lambda_0 \times 0.03\lambda_0$	15.2%	4.8	93.6%	Microstrip
Quad-resonance SIW CBS antenna in this work	10	2.2	$0.63\lambda_0 \times 1.07\lambda_0 \times 0.03\lambda_0$	17.5%	7.3	94.2%	Microstrip
Conventional SIW CBS antenna [1]	10	2.2	$0.59\lambda_0 \times 0.59\lambda_0 \times 0.02\lambda_0$	1.7%	5.4	86%	Microstrip
SIW CBS antenna using substrate removal [2]	2.45	4.4	$0.37\lambda_0 \times 0.32\lambda_0 \times 0.07\lambda_0$	2.2%	-	53.6%	Probe
SIW cavity-backed rectangular patch antenna [3]	38	2.2	$0.46\lambda_0 \times 0.77\lambda_0 \times 0.07\lambda_0$	15.6%	6.5	83.9%	SIW
SIW cavity-backed slot-patch antenna [4]	60	7.38	$0.30\lambda_0 \times 0.28\lambda_0 \times 0.22\lambda_0$	11%**	5.7**	-	Microstrip
SIW CBS antenna with resonant TCSRS [5]	28	2.2	$0.58\lambda_0 \times 0.86\lambda_0 \times 0.05\lambda_0$	16.7%	10.0	95.8%	SIW
SIW CBS antenna using hybrid modes [9]	10	2.2	$0.59\lambda_0 \times 0.41\lambda_0 \times 0.02\lambda_0$	6.3%	6.0	92.5%	Microstrip
SIW CBS antenna using hybrid modes [10]	10	2.2	$0.59\lambda_0 \times 0.53\lambda_0 \times 0.03\lambda_0$	9.4%	5.0	> 92%	Microstrip
SIW CBS antenna with 3×3 slot array [11]	33	2.2	$1.76\lambda_0 \times 1.76\lambda_0 \times 0.17\lambda_0$	> 26%	13.8	> 95%	Probe
Narrow-wall fed SIW CBS antenna [12]	35.5	10.2	$0.33\lambda_0 \times 0.54\lambda_0 \times 0.08\lambda_0$	13%**	-	-	SIW
SIW cavity-backed wide slot antenna [13]	60.5	6.15	$0.20\lambda_0 \times 0.25\lambda_0 \times 0.13\lambda_0$	11%**	-	-	SIW
SIW CBS antenna with a via-hole above the slot [15]	2.45	2.2	$0.46\lambda_0 \times 0.52\lambda_0 \times 0.01\lambda_0$	3.3%	-	-	Probe

* “CBS” is the abbreviation of “cavity-backed slot” (similarly hereinafter).

** Since the measured results were not provided, the values given here refer to the simulated results.

Fortunately, the nonradiating mode does not exactly resonate in the operation band, and therefore the antenna gain can maintain stable in the operation band. Compared with the triple-resonance design, an about 2.5 dB gain increment is obtained, due to an electrically larger SIW cavity adopted in the quad-resonance design.

Table III gives a comparison among our triple-resonance antenna, quad-resonance antenna and other previously reported SIW cavity-backed antennas. Considering the comparison between our two antennas, it is seen that the quad-resonance design achieves a 2.3% bandwidth enhancement by utilizing the additional TE_{310} mode. As compared to other antennas in [1] and [2], and especially Luo’s dual-resonance antenna without shorting vias in [9], both of our antennas yield remarkable bandwidth enhancement. Compared with the designs in [3] and [5], which have wide impedance bandwidths (11%–16.7%), high peak gains (5.65–10 dBi) and small cavity sizes, our works provide comparable fractional impedance bandwidths with a lower profile of $0.03\lambda_0$. Although the antenna in [11] has the highest gain (13.8 dBi) and the widest fractional bandwidth (>26%) in Table III, it occupies a much larger SIW cavity size of $1.76\lambda_0 \times 1.76\lambda_0 \times 0.17\lambda_0$. The efficiencies of our two antennas are above 90%, which are high among the listed designs. In summary, our proposed triple- and quad-resonance antennas exhibit simple geometries, low profile ($0.03\lambda_0$), high efficiencies (>90%), and fairly wide impedance bandwidths (15.2% and 17.5%, respectively). The sizes of the presented antennas, on the other hand, are relatively larger, when comparing with some published antennas (see [1]–[4], [9]).

VI. CONCLUSION

A triple-resonance and a quad-resonance SIW cavity-backed slot antennas have been proposed for bandwidth enhancement. The working mechanism of the triple-resonance antenna is investigated with cavity model and equivalent circuit

model analyses. For the triple-resonance antenna, a wide bandwidth is obtained by combining the lowest cavity mode to two higher modes using shorting vias. As for the quad-resonance design, a wide bandwidth is obtained by combining three lower cavity modes to a higher mode with the similar method. To verify the design concepts, prototypes of the two designs are fabricated and measured. Measured results show that the triple- and quad-resonance antennas have wide impedance bandwidths of 15.2% and 17.5%, respectively. In the bands of interest, the antennas exhibit flat gains and stable radiation patterns.

REFERENCES

- [1] G. Q. Luo, Z. F. Hu, L. X. Dong, and L. L. Sun, “Planar slot antenna backed by substrate integrated waveguide cavity,” *IEEE Antennas Wireless Propag. Lett.*, vol. 7, pp. 236–239, 2008.
- [2] S. Yun, D. Y. Kim, and S. Nam, “Bandwidth and efficiency enhancement of cavity-backed slot antenna using a substrate removal,” *IEEE Antennas Wireless Propag. Lett.*, vol. 11, pp. 1458–1461, 2012.
- [3] T. Y. Yang, W. Hong, and Y. Zhang, “Wideband millimeter-wave substrate integrated waveguide cavity-backed rectangular patch antenna,” *IEEE Antennas Wireless Propag. Lett.*, vol. 13, pp. 205–208, 2014.
- [4] K.-S. Chin, W. Jiang, W. Che, C.-C. Chang, and H. Jin, “Wideband LTCC 60-GHz antenna array with a dual-resonant slot and patch structure,” *IEEE Trans. Antennas Propag.*, vol. 62, no. 1, pp. 174–182, Jan. 2014.
- [5] P. Choubey, W. Hong, Z.-C. Hao, P. Chen, T.-V. Duong, and M. Jiang, “A wideband dual-mode SIW cavity-backed triangular-complimentary-split-ring-slot (TCSRS) antenna,” *IEEE Trans. Antennas Propag.*, vol. 64, no. 6, pp. 2541–2545, 2016.
- [6] S. Mukherjee, A. Biswas, and K. V. Srivastava, “Substrate integrated waveguide cavity-backed dumbbell-shaped slot antenna for dual-frequency applications,” *IEEE Antennas Wireless Propag. Lett.*, vol. 14, pp. 1314–1317, 2015.
- [7] S. Mukherjee, A. Biswas, and K. V. Srivastava, “Substrate integrated waveguide cavity backed slot antenna with parasitic slots for dual-frequency and Broadband Application,” in *Proc. 9th Eur. Conf. Antennas Propag. (EuCAP)*, 2015, pp. 7–11.
- [8] T. Zhang, W. Hong, Y. Zhang, and K. Wu, “Design and analysis of SIW cavity backed dual-band antennas with a dual-mode triangular-ring slot,” *IEEE Trans. Antennas Propag.*, vol. 62, no. 10, pp. 5007–5016, 2014.
- [9] G. Q. Luo, Z. F. Hu, W. J. Li, X. H. Zhang, L. L. Sun, and J. F. Zheng, “Bandwidth-enhanced low-profile cavity-backed slot antenna by using hybrid SIW cavity modes,” *IEEE Trans. Antennas Propag.*, vol. 60, no. 4, pp. 1698–1704, Apr. 2012.

- [10] S. Mukherjee, A. Biswas, and K. V. Srivastava, "Broadband substrate integrated waveguide cavity-backed bow-tie slot antenna," *IEEE Antennas Wireless Propag. Lett.*, vol. 13, pp. 1152–1155, 2014.
- [11] W. Han, F. Yang, J. Ouyang, and P. Yang, "Low-cost wideband and high-gain slotted cavity antenna using high-order modes for millimeter-wave application," *IEEE Trans. Antennas Propag.*, vol. 63, no. 11, pp. 4624–4631, Nov. 2015.
- [12] Y. Zhang, Z. N. Chen, X. Qing, and W. Hong, "Wideband millimeter-wave substrate integrated waveguide slotted narrow-wall fed cavity antennas," *IEEE Trans. Antennas Propag.*, vol. 59, no. 5, pp. 1488–1496, May 2011.
- [13] K. Gong, Z. N. Chen, X. Qing, P. Chen, and W. Hong, "Substrate integrated waveguide cavity-backed wide slot antenna for 60-GHz bands," *IEEE Trans. Antennas Propag.*, vol. 60, no. 12, pp. 6023–6026, Dec. 2012.
- [14] D. Kim, J. W. Lee, C. S. Cho, and T. K. Lee, "X-band circular ring-slot antenna embedded in single-layered SIW for circular polarisation," *Electron. Lett.*, vol. 45, no. 13, pp. 668–669, Jun. 2009.
- [15] S. Yun, D.-Y. Kim, and S. Nam, "Bandwidth enhancement of cavity-backed slot antenna using a via-hole above the slot," *IEEE Antennas Wireless Propag. Lett.*, vol. 11, pp. 1092–1095, 2012.
- [16] X.-C. Zhu *et al.*, "Design and implementation of a triple-mode planar filter," *IEEE Microw. Wireless Compon. Lett.*, vol. 23, no. 5, pp. 243–245, May 2013.
- [17] M. Rezaee and A. R. Attari, "Realisation of new single-layer triple-mode substrate-integrated waveguide and dual-mode half-mode substrate-integrated waveguide filters using a circular shape perturbation," *IET Microw. Antennas Propag.*, vol. 7, no. 14, pp. 1120–1127, Nov. 2013.
- [18] X.-C. Zhu *et al.*, "Design of a bandwidth-enhanced polarization rotating frequency selective surface," *IEEE Trans. Antennas Propag.*, vol. 62, no. 2, pp. 940–944, Feb. 2014.
- [19] J. Liu, Q. Xue, H. Wong, H. W. Lai, and Y. Long, "Design and analysis of a low-profile and broadband microstrip monopolar patch antenna," *IEEE Trans. Antennas Propag.*, vol. 61, no. 1, pp. 11–18, Jan. 2013.
- [20] J. Liu and Q. Xue, "Broadband long rectangular patch antenna with high gain and vertical polarization," *IEEE Trans. Antennas Propag.*, vol. 61, no. 2, pp. 539–546, Feb. 2013.
- [21] F. Xu and K. Wu, "Guided-wave and leakage characteristics of substrate integrated waveguide," *IEEE Trans. Microw. Theory Techn.*, vol. 53, no. 1, pp. 66–73, Jan. 2005.
- [22] J. Liu, D. R. Jackson, and Y. Long, "Substrate integrated waveguide (SIW) leaky-wave antenna with transverse slots," *IEEE Trans. Antennas Propag.*, vol. 60, no. 1, pp. 20–29, Jan. 2012.
- [23] Q. Lai, C. Fumeaux, W. Hong, and R. Vahldieck, "Characterization of the propagation properties of the half-mode substrate integrated waveguide," *IEEE Trans. Microw. Theory Techn.*, vol. 57, no. 8, pp. 1996–2004, Aug. 2009.
- [24] Y. Cassivi, L. Perregrini, P. Arcioni, M. Bressan, K. Wu, and G. Conciauro, "Dispersion characteristics of substrate integrated rectangular waveguide," *IEEE Microw. Wireless Compon. Lett.*, vol. 12, no. 9, pp. 333–335, Sep. 2002.
- [25] C. A. Balanis, *Antenna Theory-Analysis and Design*. Hoboken, NJ, USA: Wiley, 2005.
- [26] N. Marcuvitz, *Waveguide Handbook*. New York, NY, USA: McGraw-Hill, 1951.
- [27] J. R. James, P. S. Hall, and C. Wood, *Microstrip Antenna Theory and Design*. Stevenage, UK: Peregrinus, 1981.
- [28] Y. Yusuf and X. Gong, "Compact low-loss integration of High-*Q* 3-D filters with highly efficient antennas," *IEEE Trans. Microw. Theory Techn.*, vol. 59, no. 4, pp. 857–865, Apr. 2011.
- [29] X. Jiang, H. Wang, and X. Zhu, "Substrate integrated waveguide filter-antenna array with 45 degrees-inclined linear polarization," in *Proc. IEEE 4th Asia-Pacific Conf. Antennas Propag. (APCAP)*, Jun. 2015, pp. 472–473.
- [30] R. Lovato and X. Gong, "A third-order High-*Q* SIW filter/antenna with two cavities and one integrated slot antenna," in *Proc. IEEE Int. Symp. Antennas Propag. (APSURSI)*, Jun. 2016, pp. 1219–1220.
- [31] Y. Huang, T. H. Loh, L. J. Foged, Y. Lu, S. Boyes, and H. Chattha, "Broadband antenna measurement comparisons," in *Proc. 4th Eur. Conf. Antennas Propag. (EuCAP)*, Apr. 2010, pp. 1–5.



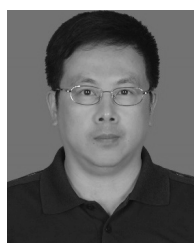
Yuzhong Shi was born in Jieyang, Guangdong, China, in 1993. He received the B.S. degree in communication engineering from Sun Yat-Sen University, Guangzhou, China, in 2016, where he is currently pursuing the M.Eng. degree.

His current research interests include microstrip antennas and substrate integrated waveguide antennas.



Juhua Liu (M'12) was born in Heyuan, Guangdong, China, in 1981. He received the B.S. and Ph.D. degrees in electrical engineering from Sun Yat-sen University, Guangzhou, China, in 2004 and 2011, respectively.

From 2008 to 2009, he was a Visiting Scholar with the Department of Electrical and Computer Engineering, University of Houston, Houston, TX, USA. From 2011 to 2012, he was a Senior Research Associate with the State Key Laboratory of Millimeter Waves, City University of Hong Kong, Hong Kong. From 2012 to 2015, he was a Lecturer with the Department of Electronics and Communication Engineering, Sun Yat-sen University, where he has been an Associate Professor since 2015. His current research interests include microstrip antennas, substrate integrated waveguide antennas, leaky-wave antennas, periodic structures, and computational electromagnetics.



Yunliang Long (M'01–SM'02) was born in Chongqing, China, in 1963. He received the B.Sc., M.Eng., and Ph.D. degrees from the University of Electronic Science and Technology of China, Chengdu, China, in 1983, 1989, and 1992, respectively.

From 1992 to 1994, he was a Post-doctoral Research Fellow and then became an Associate Professor with the Department of Electronics, Sun Yat-sen University, Guangzhou, China. From 1998 to 1999, he was a Visiting Scholar with IHF, RWTH Aachen, Aachen, Germany. From 2000 to 2001, he was a Research Fellow with the Department of Electronics Engineering, City University of Hong Kong, Hongkong. He is currently a Professor and the Head of the Department of Electronics and Communication Engineering, Sun Yat-sen University. He has authored or co-authored over 130 academic papers. His current research interests include antennas and propagation theory, electromagnetic theory in inhomogeneous lossy medium, computational electromagnetics, and wireless communication applications.

Prof. Long is a member of the Committee of Microwave Society of CIE, and is on the editorial board of the *Chinese Journal of Radio Science*. He is the Vice Chairman of Guangzhou Electronic Industrial Association. His name is listed in Who's Who in the World.